High average power 88 W OPCPA system for high-repetition-rate experiments at the LCLS x-ray free-electron laser

Katalin Mecseki,[1,*] Matthew K. R. Windeler,[1,2] Alan Miahnahri,[1] Joseph S. Robinson,[1] James M. Fraser,[2] Alan R. Fry,[1] and Franz Tavella[1]

[1]SLAC National Accelerator Laboratory, 2575 Sand Hill Road, Menlo Park, California 94025, USA
[2]Department of Physics, Engineering Physics & Astronomy, Queen's University, Kingston, Ontario, K7L 3N6, Canada
*Corresponding author: kmecseki@slac.stanford.edu

Received 10 January 2019; accepted 22 January 2019; posted 1 February 2019 (Doc. ID 357260); published 1 March 2019

We present a 100 kHz, sub-20 fs optical parametric chirped-pulse amplifier (OPCPA) system delivering 88.6 W average power at a center wavelength of 800 nm. The seed pulses are derived from the pump laser via white-light continuum generation and are amplified in three non-collinear OPCPA stages. The final two high-power stages are pumped with a 661 W Yb:YAG InnoSlab amplifier. A simple and robust design is used for the OPCPA system to avoid thermal effects and enhance long-term stability, resulting in excellent beam quality and high conversion efficiency. To the best of our knowledge, this is the highest average power OPCPA system reported to date.

Intense, ultrafast laser sources are widely deployed for pump-probe experiments at X-ray facilities such as the Linac Coherent Light Source (LCLS) X-ray free-electron laser (XFEL). LCLS-II is a planned facility upgrade that will surpass the current 120 Hz operational range, providing femtosecond X-ray pulses at a repetition rate of up to 1 MHz with initial operation at 100 kHz [1]. Pump-probe experiments will benefit from this high repetition rate with higher data rates enhancing the signal-to-noise ratio in time-resolved crystallography [2] and enabling access to "photon-hungry" measurements such as time-resolved resonant inelastic X-ray spectroscopy [3]. In order to take full advantage of these advances in the XFEL technology, the optical pump-probe laser system needs to match the XFEL repetition rate, needs to support a pulse duration shorter than <20 fs, and requires ~millijoule level pulse energies to drive secondary sources from the UV to the terahertz range. Additionally, the laser system needs to be operational 24 hours a day, seven days a week, to support user experiments at LCLS. To meet these demands, a highly engineered, robust and reliable laser system, approaching the 100 W average power level, is required.

Several technologies have been considered for high-power amplification. While conventional diode-pumped laser amplifier technology (e.g., Ti:sapphire) can reach several tens of watts of average power [4], scaling to a higher average power is challenging due to limitations caused by thermal effects in the amplifier material. Nonlinear pulse compression in gas-filled capillaries is a well-known approach for the generation of high average power, few-cycle pulses [5,6]; however, the center wavelength is tied to the center wavelength of the driver laser amplifier, the average power scaling is pulse energy limited, and sub-picosecond optical pulses are required to drive the process. Another approach is the nonlinear compression of laser pulses in gas-filled multipass cells with more than tens of millijoule energy [7–9], but only > 35 fs pulse durations have been demonstrated so far. Optical parametric chirped-pulse amplification (OPCPA), in contrast, is tunable within the phase-matching range defined by the geometry and the pump laser wavelength. Additionally, OPCPA enables the generation of high-power, high-energy and ultrashort laser pulses due to the lower heat load in the amplifier material [10]. The current state of the art systems is producing a few tens of watt average power [11–13] with, to the best of our knowledge, the highest average power OPCPA system reported to operate at 53 W average power at 1 kHz [14]. High-power, high-repetition-rate carrier-envelope phase (CEP) stable nonlinear compression in quartz plates has been recently reported, yielding > 10 W average powers [15]. Further progress in the power scaling of OPCPA systems will be possible, once few picosecond pump laser amplifiers become available with several kilowatts of average power. In this Letter, we report on a 100 kHz OPCPA system delivering 88.6 W output which, to the best of our knowledge, is the highest average power ultrafast laser source at 800 nm center wavelength to date.

The system described in this Letter consists of several commercial building blocks that are highly customized to the authors' design. The layout is presented in Fig. 1. An Yb-doped fiber oscillator seeds an Yb-doped fiber amplifier system (Tangerine, Amplitude Systemes), which is used to derive both the pump and the seed pulses for the high-power OPCPA. The oscillator repetition rate (46.4286 MHz) is chosen to be a harmonic of the XFEL repetition rate, in order to be able to synchronize the arrival of the laser pulses to the XFEL. A fraction (6 W, 6.6 nm full width at half-maximum—FWHM at 1030 nm) of the uncompressed fiber amplifier output is amplified in two stages in a diode-pumped InnoSlab amplifier (Amphos GmbH). 510 W average power, is extracted from the seven-pass, 10 mm long, longitudinally

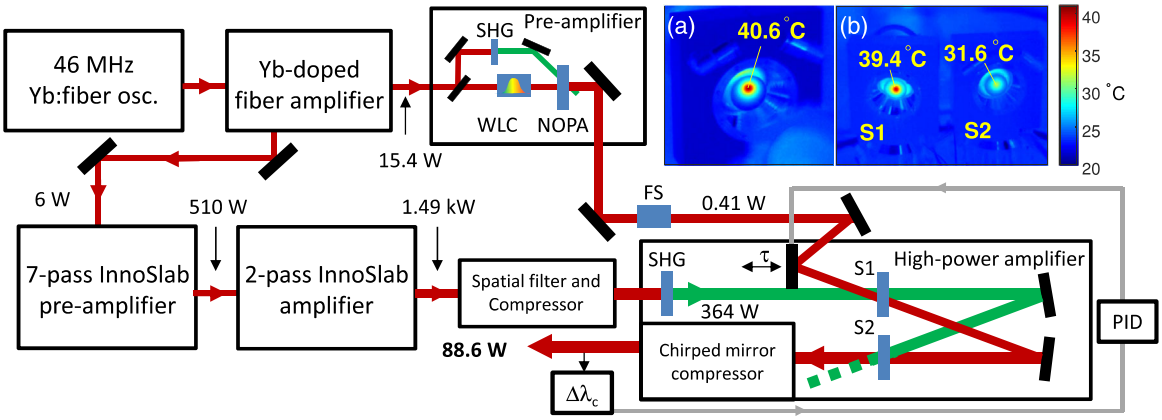

Fig. 1. Schematic of the three-stage OPCPA setup. SHG, second-harmonic generation WLC, white-light continuum; NOPA, non-collinear OPA stage; FS, fused silica stretcher; S1 and S2, high-power OPCPA stage 1 and 2. $\Delta\lambda_c$ is the measured deviation from the center wavelength, and τ represents the delay for locking the pump-signal timing with a PID-controlled feedback loop. Surface temperature measurement of (a) the 1 mm long SHG BBO crystal and (b) of the 4 mm (S1) and 2 mm (S2) OPCPA BBO crystals. The clear aperture of the crystals is 14 mm.

pumped Yb:YAG slab crystal. These pulses are subsequently amplified to 1485(±6.1) W (0.4% rms) average power in a two-pass 10 mm long Yb:YAG slab medium. A typical beam profile measured shortly after the final pass is shown in Fig. 2(b). The beam is re-shaped with a cylindrical lens system [Fig. 2(c)], and the higher-order modes are removed in a one-dimensional, spatial filter [y-coordinate on Fig. 2(c)]. The resulting beam profile is shown in Fig. 2(d) with a measured $M^2_{x/y} = 1.4/1.7$. A beam stabilization system (MRC Systems GmbH) is used to reduce the thermally induced pointing instability intrinsic to the Yb:YAG amplifier system by 90%, from $\sigma_{x/y} = 101.5/106.9$ μm to 12.9/11.4 μm (beam position variation rms, measured at the first high-power OPCPA stage). Any pointing instability during the spatial filtering leads to power fluctuations. Pulses with a spectral bandwidth of 2.7 nm FWHM are compressed in a Treacy-type grating compressor to 545 fs (531 fs Fourier limit, FWHM). The moderately inefficient compression ($\eta_c \sim 84\%$) and spatial filtering of the beam ($\eta_{sf} \sim 53\%$) limit the compressed output power of the pump to 661(±3.8) W (Ophir, 10 K-W-v3) with 0.57% rms power stability [Fig. 2(a)]. Improvements in the crystal quality and heat sink design of the kilowatt Yb:YAG amplifier crystal are expected to enhance the beam quality and reduce the spatial filtering losses. The OPCPA is operated with stretched pulses at 710 fs FWHM duration in order to increase the amplified bandwidth in the OPCPA [Fig. 2(e)]. The autocorrelation measurements of the compressed pulses are shown in Fig. 2(e). The pulses are frequency doubled in a 1 mm type-I BBO crystal with a conversion efficiency of ~55%, yielding 364(±3.4) W (0.9% rms, Ophir, L1500W-BB-v2) at 515 nm to pump the two high-power OPCPA stages. The second-harmonic beam profile recorded in the plane of the high-power OPCPA stage S1 is shown in Fig. 2(f).

The high-power OPCPA stage S1 (Fig. 1) is seeded from an OPA pre-amplifier (White Dwarf, Class 5 Photonics). The white-light continuum (WLC) seeded OPA pre-amplifier is pumped with a 15.4 W, 1030 nm fiber amplifier beam operated at 100 kHz repetition rate. The pump pulses from the fiber amplifier have a duration of 286 fs at FWHM (APE, PulseCheck, scanning second-harmonic generation [SHG] auto-correlator). A small fraction of the pump beam (208 mW) is used to generate the WLC in a 5 mm YAG slab, which is then amplified in a non-collinear OPA (NOPA) stage (5 mm, BBO crystal). Type-I phase matching in the Poynting vector walk-off compensation scheme is used. The internal non-collinear angle was chosen to be ~2.3°, the same as in the subsequent high-power OPCPA stages. The beam sizes for the seed are 1 and 1.5 mm for the pump ($1/e^2$ diameter), respectively. The pre-amplifier NOPA stage is pumped with the second-harmonic of the pump beam (8.04 W), generated in a 1 mm BBO crystal. The gain in the pre-amplifier is set to be $G < 10^3$, and the stage is kept unsaturated in order to keep a low optical parametric fluorescence background [16]. The output 413(±1.5) mW, (0.36% rms Ophir, 3A) is then further stretched in a 25 mm fused silica block in order to amplify a bandwidth that supports sub-20 fs pulses, before seeding the high-power amplification stages.

The high-power amplification takes place in a commercial two-stage OPCPA system (Supernova, Class 5 Photonics). The first (S1) and the second (S2) amplifier stages use a 4 and 2 mm type-I BBO crystals, respectively. The crystals are AR coated for 515 nm. The beam sizes are 5.5 mm ($1/e^2$ diameter). S1 has a gain of ~133, and the second stage S2 is operated at saturation with a gain of ~1.6. The overall pump-to-signal conversion efficiency is ~24.3%. The 24 h long stability measurements of the spectrum and power stability are shown in Figs. 3(a) and 3(b). In order to avoid excess idler wave absorption [12], the spectrum is kept above >700 nm. At the output, an amplified power of 88.6(±1.4) W was measured (Ophir, L1500W-BB-v2), which corresponds to a 1.6% rms stability. The optical parametric fluorescence background was measured in the absence of the seed as 3.3(±1.3) mW (Ophir, 3A). Figure 3(c) shows the seeding and the amplified spectra (OceanOptics, Flame) at the output of the pre-amplifier and after the final amplification stages. The pulses are compressed in a 14-pass chirped-mirror compressor to 16.96(±0.24) fs [Fig. 3(d)], measured with a single-shot SHG auto-correlator (using spatial beam splitting). The near-field beam profile of the amplified beam is showed in Fig. 3(e). This beam was also focused using an $f = 150$ mm off-axis parabola to 4.95 μm × 5.72 μm [Fig. 3(f)], required for future applications in LCLS-II experiments. The measured wavefront of the

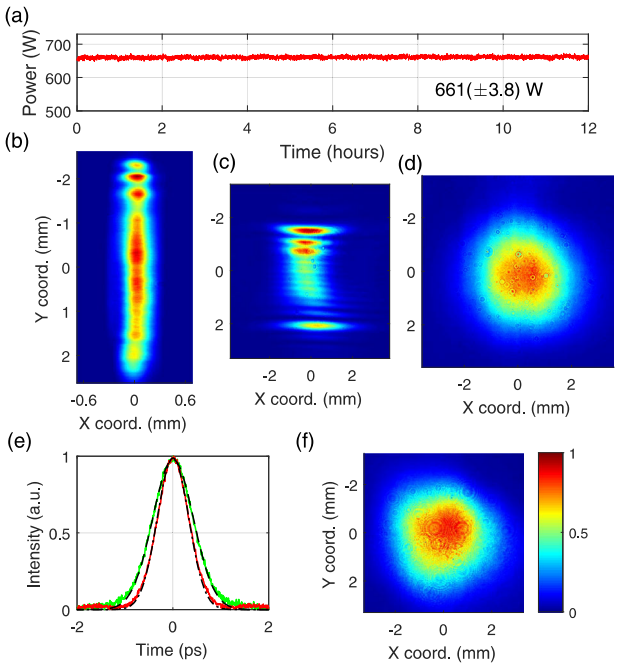

Fig. 2. High-power Yb:YAG pump amplifier parameters: (a) 12 h power measurement of the 1030 nm pump laser amplifier. (b) Spatial beam profile of the output of the two-stage high-power InnoSlab amplifier, (c) after cylindrical telescope for beam re-shaping, (d) after one-dimensional spatial filtering and the compressor. (e) Auto-correlation measurement of the pump pulses set for the OPA pump, $\tau_{\text{pump}} =$ 710 fs (green) and the compressed to near transform-limited duration, $\tau_{\text{pump}} = 545$ fs (red), assuming a Gaussian temporal pulse distribution. The fits are shown as dashed black line. (f) 515 nm pump beam profile measured in the high-power OPCPA plane (S1, Fig. 1).

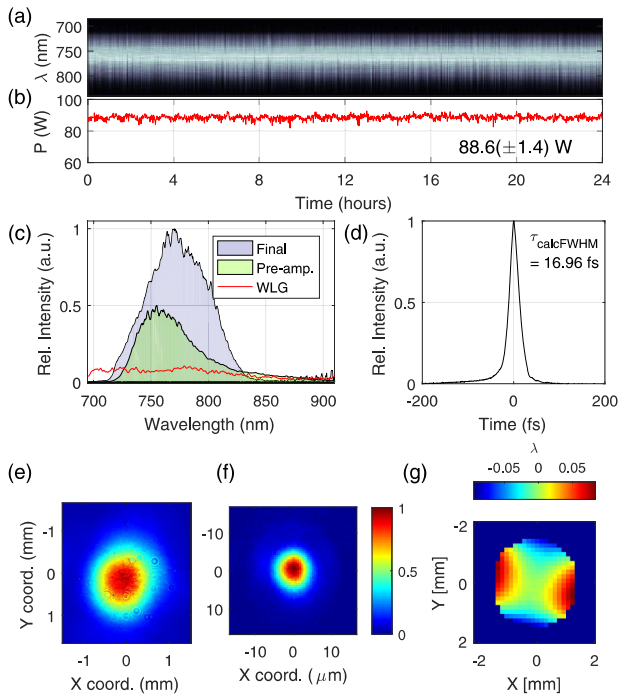

Fig. 3. High-power OPCPA parameters: (a) 24 h measurement of the amplified spectrum, linear scaling. (b) 24 h power measurement. (c) WLC spectrum (red), OPCPA pre-amplifier output spectrum (green), high-power OPCPA amplifier spectrum (blue). (d) Auto-correlation measurement, $\tau_p = 16.96$ fs, at FWHM. (e) Measured amplified near field (2.38 mm × 2.15 mm) and (f) far field (4.95 μm × 5.72 μm) beam profiles. (g) Measured wavefront at the output of the system.

compressed output (WFS40, Thorlabs) is presented in Fig. 3(g). There is negligible astigmatism in the wavefront, which is the result of a slight misalignment of the telescopes in the system to avoid damage caused by back reflections.

At significantly higher power levels than those presented in the pre-amplifier, thermal effects manifest in linear and nonlinear optical effects such as refractive index changes (the dominant second-order nonlinear effect), causing change in the phase-matching condition, and a subsequent reduction in the conversion efficiency. High temperatures and temperature gradients can additionally damage nonlinear optical materials and coatings [17–19]. Crystals and coatings with low absorption coefficients and targeted cooling schemes reduce these thermal effects in the (SHG) and the OPA crystals. A thermal image of the SHG crystal during operation is shown in Fig. 1(a) (FLIR, A655sc). The peak temperature of 40.6°C and the maximum temperature gradient of 2.7(±0.25) Kcm^{-1} are negligible for the second-harmonic conversion process, due to the high temperature acceptance of BBO. Similar measurements are performed for the seeded high-power OPCPA crystals Fig. 1(b). The difference between the peak temperature in unseeded and seeded amplifier in stage S1 and S2 is 0.8 and 2.7 K. The peak temperatures shown in Figs. 1(a) and 1(b) are 39.4° and 31.6°C and the temperature gradients are 2.0(±0.51) Kcm^{-1} and 1.0(±0.03) Kcm^{-1} for stage S1 and S2, respectively. Similar to the SHG stage, thermal effects are expected to impact the amplification process at higher temperature gradients or peak temperatures [12,17]. The temperature increases observed in our system are primarily due to pump beam absorption in the crystals.

The overall power and stability of this setup is currently limited by the pump beam parameters and can be further enhanced by improving the two-pass Yb:YAG pump crystal quality. The system presented here is designed to be safely operated with a 1.5 kW pump laser, extracting > 150 W average power. Further scaling would require a change to the stretching and compression of both the OPCPA pump and seed pulses. The physical scalability of high average power OPCPA has been studied by Riedel *et al.* [17] which, when applied to our parameters, shows that thermal dephasing for BBO would only have a significant impact at very high temperature gradients for the BBO crystal ($\Delta T >$ 150C for our parameters). Temperature gradients can be reduced, introducing high-quality crystals or introducing heat extraction techniques such as presented in Ref. [20].

The OPCPA system presented in this Letter is a prototype system. During the LCLS-II initial phase, the pump-probe laser system will be operated at an output of 40 W at 100 kHz, 20 fs. To simulate operation at this power level, the Yb:YAG two-pass InnoSlab amplifier pumped at a lower level operate marginally above transparency, resulting in ∼50% of the nominal pump power. This reduces thermal instabilities and improves the losses in the spatial filtering process before compression. While thermal instabilities contribute to pulse energy fluctuations, timing fluctuation (jitter) between the OPCPA pump and seed pulses is the major source of instability in the pulse energy. as well as the spectral and the temporal profiles. For picosecond and sub-picosecond pump pulses, timing fluctuations may cause a shift

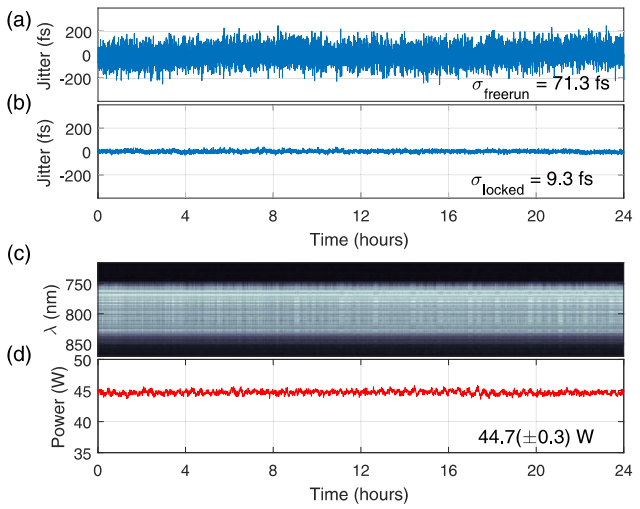

Fig. 4. 24 h measurement of the pump-signal jitter with PID locking (a) off and (b) on. 24 h (c) spectral (linear scaling) and (d) power measurement at the reduced pump power with active feedback enabled.

in the center wavelength and, in extreme cases, changes in the compressed pulse duration. For parameters presented in Fig. 3, timing fluctuations have a mean value of 71.3 fs and cause a mean center wavelength displacement of 3.3 nm [rms, spectrum in Fig. 3(a)] on a time scale of hundreds of milliseconds to seconds. The calibration of the shift of the spectral centroid due to the pump-to-signal delay is 4.615 nm per 100 fs, which was determined by varying the delay stepwise with an encoded linear stage in defined steps. A 24 h free-running pump-to-signal fluctuation measurement is presented in Fig. 4(a), where the timing fluctuations are mainly caused by residual air turbulence in the pump compressor [21,22]. These fluctuations can be compensated for by monitoring the spectrum at the output of the OPCPA and using an active proportional-integral-differential (PID) feedback loop to vary the delay shown schematically in Fig. 1. The spectral centroid is monitored at the output of the OPCPA with a home-built 4-f prism imaging spectrometer with a quadrant position detector (Thorlabs, PDQ80A) located in the Fourier plane. The signal from the spectral plane on the quadrant detector is monitored with a PID controller (Toptica, PID110), which controls the temporal delay between the pump and the signal by driving a mirror mounted on a piezo-based linear stage (Newport, NPX400). Enabling the feedback loop reduces the timing fluctuations by nearly one order of magnitude, to 9.3 fs [Fig. 4(b)]. The 24 h spectral measurement is shown in Fig. 4(c) and the corresponding power measurement in Fig. 4(d). The measured average output power is 44.7(±0.3)W (Ophir, L1500W-BB-v2). This corresponds to a 0.7% rms stability, a factor of 2 overall improvement compared to the free-running pump-to-signal fluctuations, closing the gap between OPCPA output power stability and Yb:YAG pump power stability.

To summarize, we report on a white-light seeded OPCPA system at 800 nm center wavelength, delivering sub-20 fs pulses at 88.6 W average power, corresponding to a pulse energy of 0.88 mJ at 100 kHz repetition rate. To the best of our knowledge, this is the highest average power OPCPA system presented to date. The high-power OPCPA stages are pumped with the second harmonic of an Yb:YAG InnoSlab laser at 515 nm. To further improve long-term stability, the pump-signal timing jitter is minimized by integrating a PID-controlled feedback loop into the system. Since the peak temperatures in the OPCPA crystal are low (~40°C) and the temperature gradients are small, the prospects for further increasing the output power are good, contingent on the availability of higher power pump lasers. Future laser development will also extend the output to other wavelength ranges, drive the generation of high-power secondary sources from the UV to terahertz range, and shorten the laser pulse duration via broadening in a hollow-core gas-filled capillary.

Acknowledgment. The authors thank Arvid Hage (Amphos GmbH), Torsten Mans (Amphos GmbH), Robert Riedel (Class 5 Photonics GmbH), and Michael Schulz (Class 5 Photonics GmbH) for their invaluable support during the development stage.

REFERENCES

1. T. Raubenheimer, in *Proceedings of the 36th International Free-Electron Laser Conference*, Basel (2014).
2. W. Liu, D. Wacker, C. Gati, G. W. Han, D. James, D. Wang, G. Nelson, U. Weierstall, V. Katritch, A. Barty, and N. A. Zatsepin, Science **342**, 1521 (2013).
3. P. Wernet, K. Kunnus, I. Josefsson, I. Rajkovic, W. Quevedo, M. Beye, S. Schreck, S. Grübel, M. Scholz, D. Nordlund, and W. Zhang, Nature **520**, 78 (2015).
4. S. Backus, M. Kirchner, R. Lemons, D. Schmidt, C. Durfee, M. Murnane, and H. Kapteyn, Opt. Express **25**, 3666 (2017).
5. S. Hädrich, M. Kienel, M. Müller, A. Klenke, J. Rothhardt, R. Klas, T. Gottschall, T. Eidam, A. Drozdy, P. Jójárt, and Z. Várallyay, Opt. Lett. **41**, 4332 (2016).
6. J. Rothhardt, S. Hädrich, A. Klenke, S. Demmler, A. Hoffmann, T. Gotschall, T. Eidam, M. Krebs, J. Limpert, and A. Tünnermann, Opt. Lett. **39**, 5224 (2014).
7. M. Kaumanns, V. Pervak, D. Kormin, V. Leshchenko, A. Kessel, M. Ueffing, Y. Chen, and T. Nubbemeyer, Opt. Lett. **43**, 5877 (2018).
8. M. Ueffing, S. Reiger, M. Kaumanns, V. Pervak, M. Trubetskov, T. Nubbemeyer, and F. Krausz, Opt. Lett. **43**, 2070 (2018).
9. J. Schulte, T. Sartorius, J. Weitenberg, A. Vernaleken, and P. Russbueldt, Opt. Lett. **41**, 4511 (2016).
10. H. Fattahi, H. G. Barros, M. Gorjan, T. Nubbemeyer, B. Alsaif, C. Y. Teisset, M. Schultze, S. Prinz, M. Haefner, M. Ueffing, and A. Alismail, Optica **1**, 45 (2014).
11. F. J. Furch, T. Witting, A. Giree, C. Luan, F. Schell, G. Arisholm, C. P. Schulz, and M. J. Vrakking, Opt. Lett. **42**, 2495 (2017).
12. J. Rothhardt, S. Demmler, S. Hädrich, J. Limpert, and A. Tünnermann, Opt. Express **20**, 10870 (2012).
13. M. Puppin, Y. Deng, O. Prochnow, J. Ahrens, T. Binhammer, U. Morgner, M. Krenz, M. Wolf, and R. Ernstorfer, Opt. Express **23**, 1491 (2015).
14. R. Budriūnas, T. Stanislauskas, J. Adamonis, A. Aleknavičius, G. Veitas, D. Gadonas, S. Balickas, A. Michailovas, and A. Varanavičius, Opt. Express **25**, 5797 (2017).
15. C.-H. Lu, T. Witting, A. Husakou, M. J. Vrakking, A. Kung, and F. J. Furch, Opt. Express **26**, 8941 (2018).
16. C. Homann and E. Riedle, Laser Photonics Rev. **7**, 580 (2013).
17. R. Riedel, J. Rothhardt, K. Beil, B. Gronloh, A. Klenke, H. Höppner, M. Schulz, U. Teubner, C. Kränkel, J. Limpert, and A. Tünnermann, Opt. Express **22**, 17607 (2014).
18. M. Prandolini, R. Riedel, M. Schulz, A. Hage, H. Höppner, and F. Tavella, Opt. Express **22**, 1594 (2014).
19. J. Rothhardt, S. Demmler, S. Hädrich, T. Peschel, J. Limpert, and A. Tünnermann, Opt. Lett. **38**, 763 (2013).
20. C. Rothhardt, J. Rothhardt, A. Klenke, T. Peschel, R. Eberhardt, J. Limpert, and A. Tünnermann, Opt. Mater. Express **4**, 1092 (2014).
21. S. Klingebiel, I. Ahmad, C. Wandt, C. Skrobol, S. A. Trushin, Z. Major, F. Krausz, and S. Karsch, Opt. Express **20**, 3443 (2012).
22. S. Prinz, M. Häfner, M. Schultze, C. Y. Teisset, R. Bessing, K. Michel, R. Kienberger, and T. Metzger, Opt. Express **22**, 31050 (2014).